Dexmedetomidine attenuates ferroptosis in OGD/R H9C2 cells through regulation of miR-326-5p/LCN2 axis

Sheng Huan (467620841@qq.com)
Nanjing Second Hospital
Yihao Ji
Nanjing Second Hospital
Guoping Yin
Nanjing Second Hospital

Research Article

Keywords: Ferroptosis, Myocardial ischemia-reperfusion injury, LCN2

Posted Date: March 22nd, 2022

DOI: https://doi.org/10.21203/rs.3.rs-1404634/v1

Abstract

Myocardial ischemia-reperfusion injury (IRI) is a common complication in cardiac surgery. A series of cascade reactions occurs during IRI, including apoptosis, necrosis, autophagy and focal death. Ferroptosis, a new way of programmed death, has been found play key role in IRI. Alleviating ferroptosis may be a potential direction of IRI treatment. In this study, we found mir-326-5p was differently expressed in four myocardial injury-related GEO database. Importantly, it could affect cell activity and regulate ferroptosis in oxygen-glucose deprivation/reperfusion (OGD/R) H9C2 cells via acting on its target gene LCN2. Interestingly, besides ferroptosis, we also found that mir-326-5p/LCN2 axis had a synergistic effect on inflammatory response and autophagy in OGD/R H9C2. Notably, we identified dexmedetomidine (DEX) as a natural agonist of mir-326-5p. In general, DEX significantly increased the expression of mir-326-5p and decreased the expression of LCN2 in OGD/R H9C2 cells, clearing cellular Fe2+ and inhibiting ferroptosis.

1. Background

Cardiomyocytes are sensitive to ischemia and hypoxia. Many cardiac operations, such as percutaneous coronary intervention, valve replacement and cardiac transplantation, may cause ischemia-reperfusion injury (IRI), remolding myocardial structure and impairing cardiac function[1-2]. Previous studies have shown that IRI was mainly caused by the disorder of oxygen free radical, calcium overload and activation of inflammation factors, which eventually induced cell programmed death[3]. Notably, current researches pointed out that ferroptosis may play an important role in cardiac injury[4-5]. Iron is a rich redox active metal in the body, regulating a variety of different physiological functions. The intracellular iron pool mainly exists in the form of Fe2+. When cardiomyocytes are in the state of ischemia and hypoxia for a long time, increasing intracellular Fe2+ would directly catalyze the highly expressed unsaturated fatty acids on the cell membrane, promote free atomic groups formation through Fenton reaction and expand lipid peroxidation, finally causing ferroptosis[6-8].

Lipocalin 2 (LCN2) is a member of the secretory lipoprotein family. It was originally found have antibacterial effect by binding with its receptor and influencing iron carrier in vivo, promoting iron to transport into cells and inhibiting microorganisms from obtaining iron[9]. Studies have found that LCN2 significantly increased and induced neurotoxicity when treated with exogenous iron, but decreased when treated with iron chelator deferoxamine (DFO). In addition, LCN2 also regulates inflammatory factors at the transcriptional stage, such as NF-κB, MMP9 and IL-6[10].

Non-coding RNA (including microRNA, circRNA and long-chain RNA) have been identified pivotal in pathological and physiological processes. MicroRNA, as a highly conversed RNA fraction, consists of about 20-26 bases and plays a key role in many diseases, such as myocardial injury, liver fibrosis and neurotoxicity [11].

Dexmedetomidine (DEX) is a commonly used drug to prevent intraoperative IRI. Previous studies have shown that it may maintain cell activity by inhibiting apoptosis, autophagy and focal death. It was well known that large numbers of oxygen free radicals were released during IRI, which is similar with the pathological process of ferroptosis. We hypothesized that DEX may protect cardiomyocytes from injury by inhibiting ferroptosis. However, ferroptosis related genes and specific pathways involved are still not clear. Our study aimed to explore this issue and clarified its underlying mechanism.

2. Methods

2.1 Reagent and antibody

DEX and DFO were purchased from sigma (Missouri, USA). Dulbecco's modified basic medium (DMEM), sugar free DMEM, fetal bovine serum (FBS), phosphate buffered saline (PBS) and trypsin EDTA were purchased from GIBCO (New York, USA). The primary antibody against β-actin (CL594-66009) and LCN2 (26991-1-AP) were purchased from Proteintech (Chicago, Illinois). The primary antibodies against p62 (#A19700), Beclin-1(#A7353), LC3B (#A19665), MMP9 (#A0289), Bax (#A19684), Bcl-2 (#A19693) and NF-KB (#A19653) were purchased from Abclonal (Wuhan, China). The plasmids of LCN2 was designed by Kaiji Biological Company (Nanjing, China). Mir-326-5p mimic and mir-326-5p inhibitor were designed and constructed by Jima Biological Company (Shanghai, China).

2.2 Cell culture

H9C2 cells were purchased from Sciences Cell Bank of Chinese Academy (Shanghai, China). The cells were cultured in DMEM containing 10% fetal bovine serum (FBS) and 1% antibiotics at 37 ° C in a humidified incubator with 5% CO2. Cell morphology was evaluated using an inverted microscope by the ZEISS system (ZEISS, USA).

2.3 Establishment of OGD/R model

The model was established with reference to the literature and slightly modified.

DMEM was cleared and the 96-well plate was washed by PBS for three times. Sugar free DMEM without FBS was added instead. Then the plate was placed in anaerobic bag (Mitsubishi, Japan) at 37°C in humidified incubator for 3, 6, 9 and 12 hours. When the scheduled time is reached, we discarded sugar free DMEM and washed the 96-well plate with PBS for three times. Complete DMEM with 10% FBS was added and the cells was cultured in normal condition for 1, 3, 6 and 9 hours.

2.4 Plasmid transfection

According to Lipofectamine 2000 instructions (Thermo Fisher, USA), H9C2 cells were transfected with corresponding siRNA or miRNA plasmid.

2.5. Real-time PCR

We lysed H9C2 cells with Trizol reagent (Life Technologies, MA, USA). Then we precipitated the total RNA with isopropanol (Aladdin, Shanghai, China) and transcribed to cDNA according to the instructions of HifairII 1st Strand cDNA Synthesis SuperMix (YEASEN, Shanghai, China). Finally, we performed real-time PCR with Hieff™ qreal-time PCR SYBR Green Master Mix (Low Rox Plus) (YEASEN, Shanghai, China) in Applied Biosystems 7500 machine (Thermo Fisher, MA, USA) following the manufacturer's guidelines.

2.7. Western Blot

Protein of each sample was extracted and added with the same account. Then it was separated by SDS-PAGE and transferred to PVDF membrane. After blocking with 5% BSA, the PVDF membrane was incubated with corresponding primary antibody overnight. HRP bound secondary anti-rabbit was applied for 2 hours next. The PVDF membrane was added with ECL (YEASEN, Shanghai, China) and protein stripe was analyzed by Image Lab software.

2.8 Immunofluorescence assay

H9C2 cells were inoculated on the cover glass in 24-well plate. After clearing DMEM, the cell morphology was fixed with 4% paraformaldehyde for 20 minutes and penetrated by 0.1 % Triton. Then it was blocked by 1% bovine serum albumin for 2 hours and incubated with primary antibody overnight. FITC rabbit secondary antibody was added for 2 hours. Then, 2ul fluorescence quencher was added on the cover glass. All images were taken blindly with Zeiss microscope (Germany).

2.9 Malondialdehyde (MDA) assays

According to the instructions, H9C2 cells were intervened with MDA working solution from Jiancheng Bioengineering Institute (Nanjing, China). MDA concentration was determined at 532 nm by microplate reader.

2.10 Iron ion detection

The Fe2+ level in H9C2 cells was detected using Iron detection kit (ferrozine microplate method) from Yita biotech company (Beijing, China) according to the manufacturer's instructions.

2.11 Mitochondrial membrane potential detection

Mitochondrial membrane potential level was detected using mitochondrial membrane potential test kit (JC-1 method) from Yita biotech company (Beijing, China). Pictures was taken under the fluorescence microscope and fluorescence intensity was measured using Synergy HTX Multi-Mode Microplate Reader (Agilent, USA) with excitation/emission wavelength of 490 nm/530 nm and 525 nm/590 nm.

2.12 Oxygen free radical (ROS) assay

According to the guidelines, H9C2 cells were intervened with ROS working solution from Jiancheng Bioengineering Institute (Nanjing, China). The fluorescence intensity was measured with

excitation/emission wavelength of 488 nm/525 nm.

2.13 Superoxide dismutase (SOD assay

According to the instructions, H9C2 cells were intervened with SOD working solution from Jiancheng Bioengineering Institute (Nanjing, China). SOD concentration was determined at 450 nm by microplate reader.

2.14 Luciferase assay

H9C2 cells were transfected with mir-326-5p mimics and WT or MUT psiCHECK2-LCN2. After 24 hours, the cells were lysed on ice and added with firefly luciferase detection reagent according to the instructions. Then the samples were measured using Synergy HTX Multi-Mode Microplate Reader.

2.15 Cell Counting Kit-8 (CCK-8) assay

H9C2 cells were plated in 96-well plates for different intervention for 24 hours. Then, 10μl CCK8 reagent was added and incubated at 37°C for 4h. The results were determined by microplate reader at 450 nm.

2.16 MTT Assay

H9C2 cells were plated in 96-well plates for different intervention. 10μl MTT reagent was added and incubated at 37°C for 4h. Then DMSO was added to dissolve the formazan. The results were determined by microplate reader at 592 nm.

2.17 Statistics

Results was expressed as mean ± standard deviation and mapped with graphpad prism 7.0 (graphpad software, San Diego, California). Statistical analysis was determined by one-way ANOVA of Student t-test (comparison between two groups) or student Newman Keuls test (more than two groups). The value of $P < 0.05$ was considered statistically significant.

3. Results

3.1 Establishment of OGD/R model and identification of ferroptosis

We set up different time of OGD for 3, 6, 9, 12 hours and different time of reperfusion for1, 3, 6, 9 hours. Compared with control group, results of CCK8 and MTT assay showed that the cell viability treated with OGD decreased significantly with the extension of OGD time. The cell viability decreased to less than 40% at OGD 12h and about 50% at OGD 9h. We chose 9h as the OGD model time in order to leave more space for next intervention. Compared with OGD9/R0 group, cell viability decreased after reperfusion of 1 hour and 3 hours, while slightly increasing at the point of 6 and 9 hours. (Fig 1A and 1B) Therefore, OGD 9h/R 3h was chosen as the most suitable model time. Under light microscope, the cells in control group were

spindle shaped and cell membrane surface was smooth and arranged neatly. However, the cells appeared empty and retracted in model groups. In addition, cells number also decreased significantly. (Fig 1C)

The results of iron ion kit showed that the Fe2+ in OGD/R group was significantly higher than that in control group, but partly decreased after treatment of DFO. (Fig 1D) In addition, SOD assay showed that SOD level decreased after OGD/R intervention but partly increased after DFO treatment. (Fig 1E) MDA assay showed that MDA level increased after OGD/R intervention but partly decreased after DFO treatment. (Fig 1F) JC-1 fluorescence assay showed that mitochondrial membrane potential level decreased after OGD/R intervention but partly increased after DFO treatment. (Fig 1G) ROS fluorescence assay showed that ROS level increased after OGD/R intervention but partly decreased after DFO treatment. (Fig 1H)

3.2 Mir-326-5p upregulation decreased ferroptosis in OGD/R H9C2

We analyzed four myocardial injury related GEO databases（GEO36239, GEO95855, GEO44179, GEO143168）. The results showed that there were significant differences in the expression of rno-mir-532, rno-mir-345, rno-mir-34a, rno-mir-18a and rno-mir-326. (Fig 2A) Since KEGG enrichment analysis showed that only the target genes of mir-326 were enriched in pathway of ferroptosis, we would like to explore the role of mir-326-5p in ferroptosis of myocardial injury. (Supplementary Fig 1)

Real-time PCR results showed that mir-326-5p mimic and inhibitor were successfully transfected into H9C2 cells. (Supplementary Fig 2) Iron ion kit showed that mir-326-5p could decreased intracellular Fe2+ in OGD/R H9C2 cells while inhibitor could increase it. (Fig 2B) MTT assay also confirmed that overexpression of mir-326-5p increased cell viability. (Fig 2C) Moreover, SOD assay showed that overexpression of mir-326-5p increased the level of SOD but knockdown of mir-326-5p decreased it. (Fig 2D) MDA assay also revealed that overexpression of mir-326-5p decreased the level of MDA but knockdown of mir-326-5p increased it. (Fig 2E) In conclusion, mir-326-5p upregulation could clear intracellular Fe2+ and protect OGD/R H9C2 cells from oxidative stress injury.

3.3 Mir-326-5p targeted LCN2 and repressed its expression

In order to further clarify the mechanism of mir-326-5p regulating ferroptosis, we searched potential targets of mir-326-5p. With the help of Targetscan (version 7.2), we found that LCN2 has the highest weighted context + + score among the target genes of mir-326-5p; while mir-326-5p has the second highest target score among the upstream miRNA of LCN2. Other prediction software also confirmed the targeting relationship between LCN2 and mir-326-5p. Therefore, we hypothesized that mir-326-5p may directly bind with LCN2 to regulate ferroptosis. （Supplementary Fig 3）

Real-time PCR and WB results showed that mir-326-5p mimic reduced mRNA and protein of LCN2 of H9C2, while inhibitor increased it. (Fig 3A and 3B) The primers sequence of LCN2 used for real-time PCR was lister in Supplementary Table 1. Immunofluorescence and DAPI staining revealed that in normal H9C2 cells, mir-326-5p mimic decreased the expression of LCN2, while inhibitor increased its expression.

(Fig 3C) Luciferase assay showed that fluorescence level of WT psiCHECK2-LCN2 but not MUT psiCHECK2-LCN2 was significantly decreased by rno-mir-326-5p mimic, confirming that LCN2 was the direct target of mir-326-5p. (Fig 3D) Real-time PCR results showed that the mRNA expression of LCN2 in OGD/R group was significantly higher than that in control group, while expression of mir-326 significantly decreased. This condition was partly reversed after DFO intervention. (Fig 3E and 3F) WB results also confirmed the significant changes in protein expression of LCN2 between groups of OGF, OGD/R and OGD/R+DFO. (Fig 3G)

3.4 Axis of mir-326-5p/LCN2 regulated ferroptosis, autophagy and inflammatory response in OGD/R H9C2

Real-time PCR and WB results showed that LCN2 siRNA was successfully transfected into H9C2 cells. (Fig 4 and Supplementary Fig 4) The results of iron ion kit showed that the Fe2+ level decreased significantly after LCN2 siRNA intervention, which was conversed by mir-326-5p inhibitor. (Fig 4A) SOD and MDA experiments also confirmed that SOD increased and MDA decreased after LCN2 siRNA intervention, which was conversed by mir-326-5p inhibitor. (Fig 4B-C) JC-1 fluorescence experiment and ROS fluorescence experiment showed that mitochondrial membrane potential level increased and ROS level decreased after LCN2 siRNA intervention, which was reversed by mir-326-5p inhibitor. (Fig 4D-E) Combined with our previous experimental results, we concluded that mir-326-5p reduced the ferroptosis of OGD/R by negatively regulating LCN2. In addition, we also found that LCN2 siRNA reduced the expression of inflammatory factors MMP9 and NF-KB, and simultaneous decreased the autophagy level by decreasing autophagy related marker proteins Beclin-1 and LC3b and increasing p62. Mir-326-5p inhibitor could partly reversed its function of inhibiting inflammatory reaction and autophagy by negatively regulating LCN2. (Fig 4F)

3.5 DEX treatment attenuated ferroptosis via mir-326-5p/LCN2 axis

Previous studies have shown that DEX could significantly reduce IRI. In order to further explore the mechanism of DEX in protecting cardiomyocytes from IRI. We intervened the H9C2 cells with 1.0 mM DEX before OGD/R. Real-time PCR results showed that mir-326-5p of OGD/R H9C2 treated with DEX increased significantly while LCN2 mRNA decreased significantly. (Fig 5A) The protein level of LCN2 decreased significantly after DEX treatment while increasing after mir-326-5p inhibitor intervention. (Fig 5B) Iron ion kit showed that DEX treatment could decrease intracellular Fe2+ in OGD/R H9C2 cells while inhibitor increased it. (Fig 5C)

In addition, SOD and MDA experiments also confirmed that SOD increased and MDA decreased after DEX treatment, which was conversed by mir-326-5p inhibitor. (Fig 5D-E) JC-1 fluorescence experiment and ROS fluorescence experiment showed that mitochondrial membrane potential level increased and ROS level decreased after DEX treatment, which was reversed by mir-326-5p inhibitor. (Fig 5F-G) All above results confirmed that DEX may inhibit ferroptosis in OGD/R H9C2 via regulating mir-326-5p.

4. Discussion

The pathogenesis of ischemia-reperfusion is complex. How to prevent IRI has been a difficult problem in the field of anesthesia. It is a comprehensive process of various noxious stimulation, including oxygen free radical release, calcium overload, leukocyte activation and lack of high-energy phosphate compounds. At present, great progress has been made in IRI prevention, such as ischemic preconditioning, ischemic postconditioning or drug intervention [12-13]. Dexmedetomidine, as a β_2 adrenergic agonists, has been proved positive effect on IRI. Previous studies have proved that it may protect cell activity and maintain organ function by inhibiting cellular apoptosis, autophagy, focal death or necrotic apoptosis. However, whether it can regulate ferroptosis and the specific mechanism have not been explored and discussed [14].

OGD/R is often used as cell model of IRI. In our experiment, when OGD time reached 9 hours, cell death occurred in about 50% of cardiomyocyte. Cell viability reached the lowest level after three hours of reoxygenation. Therefore, we chose OGD9/R3 as the modeling time. Our results also showed that after OGD/R intervention, intracellular Fe2+, ROS and MDA increased significantly, and SOD decreased significantly. In addition, remarkable changes also happened in the mitochondrial membrane potential, proving that OGD/R could induce ferroptosis in H9C2 cells.

The intracellular iron plays an important role in maintaining cellular homeostasis[15-16]. However, excessive iron may cause series of cellular reactions, including oxidative stress, mitochondrial dysfunction and endoplasmic reticulum stress. Iron ion is mainly absorbed in the duodenum through divalent metal ion transporter 1 (DMT-1) and heme carrier protein 1 (HCP-1). Iron ion in the cytoplasm can be stored as ferritin or released into the blood through iron transporter (FPN)[17-18]. When transferrin (TF) mediated classical iron transporting reaches saturation, iron starts entering cells through a non-TF binding pathway, including DMT-1, T-type calcium channel (TTCC), L-type calcium channel (LTCC)[19-20]. LCN2 has also been found bind to LCN2 receptor and influence iron carrier on the surface of cell membrane, significantly increasing the content of intracellular iron as an additional access[21-22].

Previous studies have recorded the continuous occurrence of LCN2 in heart that LCN2 starts from epicardium to myocardium, and finally arrived in endocardium. In fact, several studies have reported that LCN2 increased in various heart disease. The level of LCN2 was also negatively correlated with the degree of disease and prognosis[23]. In chronic heart failure (CHF) patients, stronger LCN2 immunostaining was observed in cardiomyocytes. Expression of LCN2 in serum was also associated with the NYHA grade and N-terminal pro-brain natriuretic peptide (NT-proBNP)[24-25]. According to our research results, abnormal aggregation of LCN2 in myocardium may increase intracellular Fe2+ and oxidative stress, finally causing ferroptosis, and this condition could be reversed by its upstream mir-326-5p. This was also consistent with the phenomenon that many clinical trial found LCN2 in serum and myocardium acted as a predictive biomarker and increased in cardiac disease.

In animal experiments, , LCN2 mRNA in aorta and myocardium of atherosclerotic mice was higher than that of normal mice after 48 hours of exposure to hypoxic environment. Pathological sections also confirmed that LCN2 protein was abundant in the myocardial and lipid core of arterial plaque, which was co-located with MMP-9[26-27]. In the rat autoimmune myocarditis model, the increased myocardial and plasma LCN2 were more obvious in the active stage of myocarditis, which may be related to myocardial and plasma IL-1β[28].

Studies over the past decade have verified that miRNA played a crucial role in many aspects of life activity. MiRNA targeted therapy is also moving from experiment to clinic trail. For example, the tumor suppressor miRNA miR-34 mimic encapsulated in lipid nanoparticles was the most advanced miRNA therapy. At present, it has been applied in the phase I clinical trial of several tumors and hematological diseases (NCT01829971). In addition, the treatment of locked nuclear acids (LNA) inhibiting miR-122 has also been used in phase II clinical trials for the treatment of hepatitis[29-30]. MiRNA targeted therapy has a wide application prospect [31]. We found that mir-326-5p is a co-expressed differential miRNA in multiple myocardial injury related GEO databases, and its target genes are mainly enriched in ferroptosis, lipid metabolism and vesicular transport. LCN2 is the direct target of mir-326-5p. Our study confirmed the mir-326/LCN2 axis could regulate ferroptosis in myocardium injury. Silencing LCN2 can significantly reduce the content of intracellular Fe2+, ROS, MDA and mitochondrial membrane potential disorder. Moreover, it could also inhibit autophagy in OGD/R H9C2 cells and reduce the expression of inflammatory factors MMP9 and NF-KB.

In conclusion, our results confirmed for the first time that DEX influenced the ferroptosis in OGD/R H9C2 cells through mediating mir-326-5p/LCN2 axis, and confirmed that LCN2 knockdown could alleviate inflammatory reaction and inhibit autophagy simultaneous. This study explored the mechanism of ferroptosis in the process of myocardial injury, providing a new perspective and target for the prevention of myocardial ischemia-reperfusion.

Declarations

Ethics approval and consent to participate

We confirmed that all methods were carried out in accordance with relevant guidelines and regulations.

Consent for publication

Not applicable.

Availability of data and materials

The datasets used and/or analyzed during the current study available from the corresponding author on reasonable request.

Competing interests

We declared that we had no conflict of interest.

Authors' contributions

Sheng Huan and Guoping Yin contributed to the conception of the study;

Sheng Huan and Yihao Ji performed the experiment;

Sheng Huan and Guoping Yin contributed significantly to data analysis and manuscript preparation;

All authors performed resources, supervision, original draft writing.

Funding

This work was supported in part by the Natural Science Foundation of Nanjing University of traditional Chinese medicine (XZR2020072) and Graduate Research and Innovation Projects of Jiangsu Province (KYCX21_1637).

Acknowledgements

We are very grateful for the help provided by the experiment center for science and technology of Nanjing University of Chinese Medicine.

References

1. Q. Zhou, J. Deng, J. Yao, J. Song, D. Meng, Y. Zhu, M. Xu, Y. Liang, J. Xu, J.P. Sluijter, J. Xiao, Exercise downregulates HIPK2 and HIPK2 inhibition protects against myocardial infarction, EBioMedicine, 74 (2021) 103713.
2. Q. Shao, J. Xia, P. Wu, J. Ying, Dexmedetomidine protects cardiac microvascular endothelial cells from the damage of ogd/r through regulation of the pparδ-mediated autophagy, Microcirculation (New York, N.Y. : 1994), 28 (2021) e12675.
3. J. Zhao, Z. Cheng, X. Quan, Z. Xie, L. Zhang, Z. Ding, Dimethyl fumarate protects cardiomyocytes against oxygen-glucose deprivation/reperfusion (OGD/R)-induced inflammatory response and damages via inhibition of Egr-1, International immunopharmacology, 86 (2020) 106733.
4. W. Li, W. Li, Y. Leng, Y. Xiong, Z. Xia, Ferroptosis Is Involved in Diabetes Myocardial Ischemia/Reperfusion Injury Through Endoplasmic Reticulum Stress, DNA and cell biology, 39 (2020) 210-225.
5. N. Li, W. Wang, H. Zhou, Q. Wu, M. Duan, C. Liu, H. Wu, W. Deng, D. Shen, Q. Tang, Ferritinophagy-mediated ferroptosis is involved in sepsis-induced cardiac injury, Free radical biology & medicine, 160 (2020) 303-318.
6. H. Nishizawa, M. Matsumoto, T. Shindo, D. Saigusa, H. Kato, K. Suzuki, M. Sato, Y. Ishii, H. Shimokawa, K. Igarashi, Ferroptosis is controlled by the coordinated transcriptional regulation of

glutathione and labile iron metabolism by the transcription factor BACH1, The Journal of biological chemistry, 295 (2020) 69-82.

7. T. Tadokoro, M. Ikeda, T. Ide, H. Deguchi, S. Ikeda, K. Okabe, A. Ishikita, S. Matsushima, T. Koumura, K.I. Yamada, H. Imai, H. Tsutsui, Mitochondria-dependent ferroptosis plays a pivotal role in doxorubicin cardiotoxicity, JCI insight, 5 (2020).
8. X. Chen, X. Li, X. Xu, L. Li, N. Liang, L. Zhang, J. Lv, Y.C. Wu, H. Yin, Ferroptosis and cardiovascular disease: role of free radical-induced lipid peroxidation, Free radical research, 55 (2021) 405-415.
9. K. Pinyopornpanish, N. Chattipakorn, S.C. Chattipakorn, Lipocalin-2: Its perspectives in brain pathology and possible roles in cognition, Journal of neuroendocrinology, 31 (2019) e12779.
10. R.F. Siciliano, D.M. Gualandro, M.S. Bittencourt, M. Paixão, F. Marcondes-Braga, A.M. Soeiro, C. Strunz, A.P. Pacanaro, C. Puelacher, F. Tarasoutchi, S. Di Somma, B. Caramelli, M.T. de Oliveira Junior, A.J. Mansur, C. Mueller, A.C.P. Barretto, T.M.V. Strabelli, Biomarkers for prediction of mortality in left-sided infective endocarditis, International journal of infectious diseases : IJID : official publication of the International Society for Infectious Diseases, 96 (2020) 25-30.
11. L.N. Lin, Q.M. Zhang, Y.Y. Ge, B. Luo, X.X. Xie, A Review of miR-326 and Female Related Diseases, Acta histochemica et cytochemica, 54 (2021) 79-86.
12. T. Li, Y. Tan, S. Ouyang, J. He, L. Liu, Resveratrol protects against myocardial ischemia-reperfusion injury via attenuating ferroptosis, Gene, 808 (2022) 145968.
13. Q. Zhang, J. Shi, D. Guo, Q. Wang, X. Yang, W. Lu, X. Sun, H. He, N. Li, Y. Wang, C. Li, W. Wang, Qishen Granule alleviates endoplasmic reticulum stress-induced myocardial apoptosis through IRE-1-CRYAB pathway in myocardial ischemia, Journal of ethnopharmacology, 252 (2020) 112573.
14. M. Conrad, B. Proneth, Broken hearts: Iron overload, ferroptosis and cardiomyopathy, Cell research, 29 (2019) 263-264.
15. M. Kobayashi, T. Suhara, Y. Baba, N.K. Kawasaki, J.K. Higa, T. Matsui, Pathological Roles of Iron in Cardiovascular Disease, Current drug targets, 19 (2018) 1068-1076.
16. H. Imai, M. Matsuoka, T. Kumagai, T. Sakamoto, T. Koumura, Lipid Peroxidation-Dependent Cell Death Regulated by GPx4 and Ferroptosis, Current topics in microbiology and immunology, 403 (2017) 143-170.
17. H. Wang, P. An, E. Xie, Q. Wu, X. Fang, H. Gao, Z. Zhang, Y. Li, X. Wang, J. Zhang, G. Li, L. Yang, W. Liu, J. Min, F. Wang, Characterization of ferroptosis in murine models of hemochromatosis, Hepatology (Baltimore, Md.), 66 (2017) 449-465.
18. T.J. Park, J.H. Park, G.S. Lee, J.Y. Lee, J.H. Shin, M.W. Kim, Y.S. Kim, J.Y. Kim, K.J. Oh, B.S. Han, W.K. Kim, Y. Ahn, J.H. Moon, J. Song, K.H. Bae, D.H. Kim, E.W. Lee, S.C. Lee, Quantitative proteomic analyses reveal that GPX4 downregulation during myocardial infarction contributes to ferroptosis in cardiomyocytes, Cell death & disease, 10 (2019) 835.
19. S. Tsurusaki, Y. Tsuchiya, T. Koumura, M. Nakasone, T. Sakamoto, M. Matsuoka, H. Imai, C. Yuet-Yin Kok, H. Okochi, H. Nakano, A. Miyajima, M. Tanaka, Hepatic ferroptosis plays an important role as

the trigger for initiating inflammation in nonalcoholic steatohepatitis, Cell death & disease, 10 (2019) 449.

20. V. Musolino, S. Palus, C. Latouche, M. Gliozzi, F. Bosco, F. Scarano, S. Nucera, C. Carresi, M. Scicchitano, S. von Haehling, F. Jaisser, G. Hasenfuss, S.D. Anker, V. Mollace, J. Springer, Cardiac expression of neutrophil gelatinase-associated lipocalin in a model of cancer cachexia-induced cardiomyopathy, ESC heart failure, 6 (2019) 89-97.
21. M.H. Roudkenar, R. Halabian, A.M. Roushandeh, M.R. Nourani, N. Masroori, M. Ebrahimi, M. Nikogoftar, M. Rouhbakhsh, P. Bahmani, A.J. Najafabadi, M.A. Shokrgozar, Lipocalin 2 regulation by thermal stresses: protective role of Lcn2/NGAL against cold and heat stresses, Experimental cell research, 315 (2009) 3140-3151.
22. E. Vafadarnejad, G. Rizzo, L. Krampert, P. Arampatzi, A.P. Arias-Loza, Y. Nazzal, A. Rizakou, T. Knochenhauer, S.R. Bandi, V.A. Nugroho, D.J.J. Schulz, M. Roesch, P. Alayrac, J. Vilar, J.S. Silvestre, A. Zernecke, A.E. Saliba, C. Cochain, Dynamics of Cardiac Neutrophil Diversity in Murine Myocardial Infarction, Circulation research, 127 (2020) e232-e249.
23. S. Lee, M.K. Jha, K. Suk, Lipocalin-2 in the Inflammatory Activation of Brain Astrocytes, Critical reviews in immunology, 35 (2015) 77-84.
24. L. Recinella, G. Orlando, C. Ferrante, A. Chiavaroli, L. Brunetti, S. Leone, Adipokines: New Potential Therapeutic Target for Obesity and Metabolic, Rheumatic, and Cardiovascular Diseases, Frontiers in physiology, 11 (2020) 578966.
25. A.R. Moschen, T.E. Adolph, R.R. Gerner, V. Wieser, H. Tilg, Lipocalin-2: A Master Mediator of Intestinal and Metabolic Inflammation, Trends in endocrinology and metabolism: TEM, 28 (2017) 388-397.
26. A.I. Cabedo Martinez, K. Weinhäupl, W.K. Lee, N.A. Wolff, B. Storch, S. Żerko, R. Konrat, W. Koźmiński, K. Breuker, F. Thévenod, N. Coudevylle, Biochemical and Structural Characterization of the Interaction between the Siderocalin NGAL/LCN2 (Neutrophil Gelatinase-associated Lipocalin/Lipocalin 2) and the N-terminal Domain of Its Endocytic Receptor SLC22A17, The Journal of biological chemistry, 291 (2016) 2917-2930.
27. X. Xiao, B.S. Yeoh, P. Saha, R.A. Olvera, V. Singh, M. Vijay-Kumar, Lipocalin 2 alleviates iron toxicity by facilitating hypoferremia of inflammation and limiting catalytic iron generation, Biometals : an international journal on the role of metal ions in biology, biochemistry, and medicine, 29 (2016) 451-465.
28. A. Urbschat, A.K. Thiemens, C. Mertens, C. Rehwald, J.K. Meier, P.C. Baer, M. Jung, Macrophage-secreted Lipocalin-2 Promotes Regeneration of Injured Primary Murine Renal Tubular Epithelial Cells, International journal of molecular sciences, 21 (2020).
29. Zhang L., Liao Y., and Tang L, MicroRNA-34 family: a potential tumor suppressor and therapeutic candidate in cancer, Journal of experimental & clinical cancer research : CR 38, 53 (2019).
30. Rupaimoole R.. and Slack F.J, MicroRNA therapeutics: towards a new era for the management of cancer and other diseases, Nature reviews Drug discovery, 16 (2017) 203-222.

31. van Rooij E.. and Kauppinen S. Development of microRNA therapeutics is coming of age, EMBO molecular medicine, 6 (2014) 851-864.

Figures

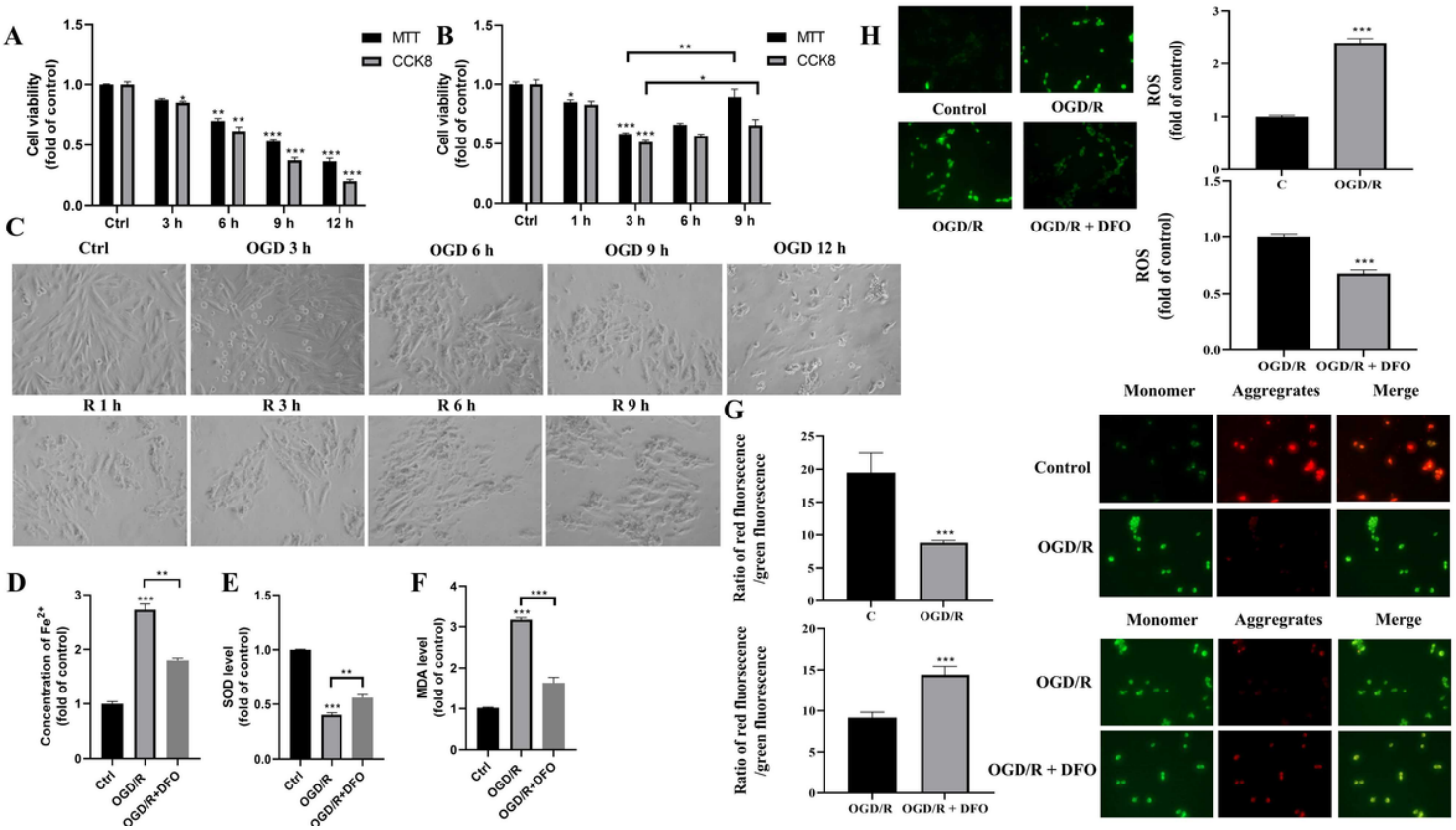

Figure 1

Establishment of OGD/R model and identification of ferroptosis. (A) Cell viability of OGD H9C2 detected by MTT and CCK8 assay. (B) Cell viability of OGD/R H9C2 detected by MTT and CCK8 assay. (C) Cell morphology photographed under light microscope. (D) Detection of Fe2+ concentration in H9C2 treated with OGD/R and DFO. (E) Detection of SOD level in H9C2 treated with OGD/R and DFO. (F) Detection of MDA level in H9C2 treated with OGD/R and DFO. (G)Fluorescence staining of JC-1 in H9C2 treated with OGD/R and DFO. (green fluorescent represents JC-1 monomers and red fluorescent represents JC-1 aggregate forms). (H) Fluorescence staining of ROS in H9C2 treated with OGD/R and DFO.

Data are expressed as mean ± SD (n = 3); *P < 0.05, **P < 0.01, ***P < 0.001.

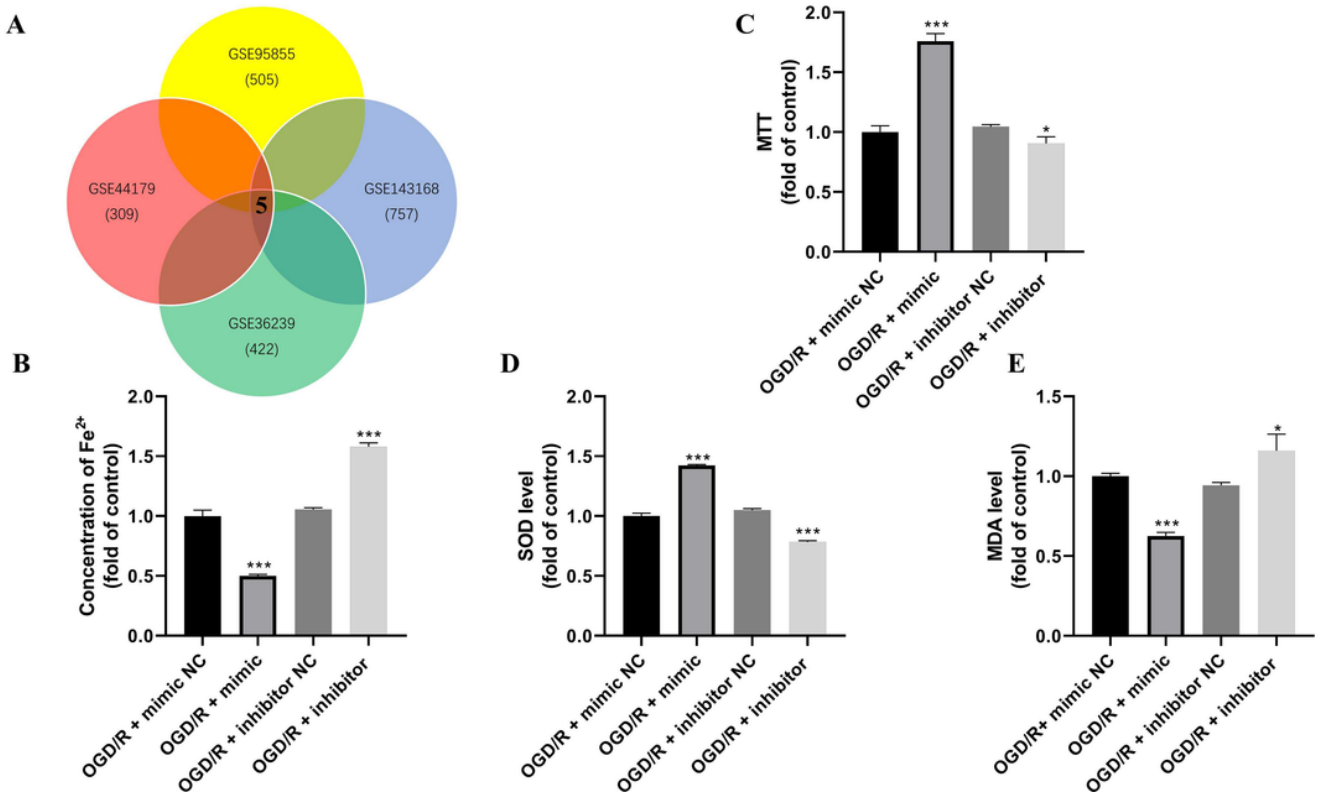

Figure 2

Mir-326-5p upregulation decreased ferroptosis in OGD/R H9C2. (A) Differential genes in four GEO databases. (B) Cell viability of OGD H9C2 detected by MTT assay. (C) Detection of Fe2+ concentration in H9C2 treated with mir-326-5p mimic and mir-326-5p inhibitor. (D) Detection of SOD level in H9C2 treated with mir-326-5p mimic and mir-326-5p inhibitor. (E) Detection of MDA level in H9C2 treated with mir-326-5p mimic and mir-326-5p inhibitor.

Data are expressed as mean ± SD (n = 3); *P < 0.05, **P < 0.01, ***P < 0.001.

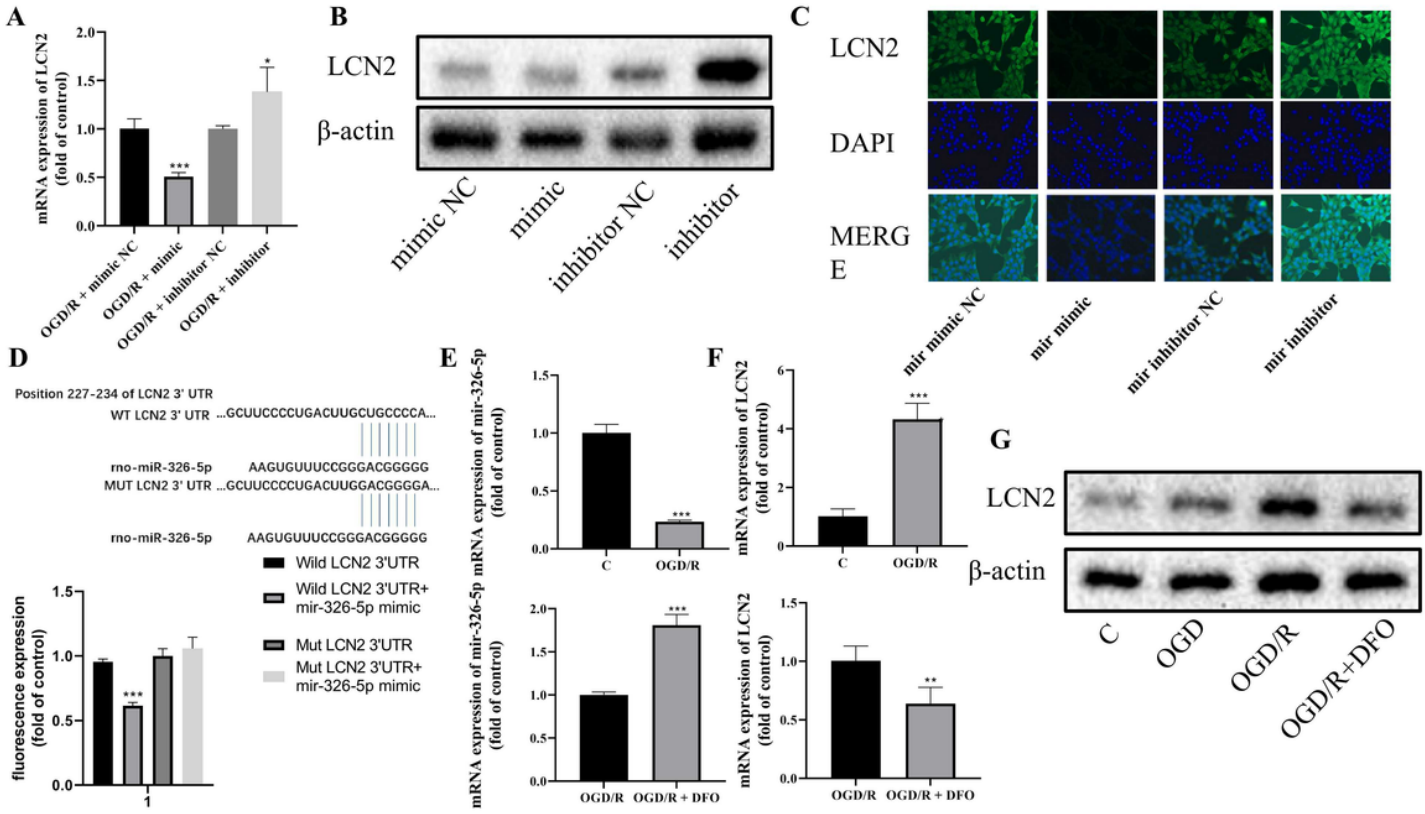

Figure 3

Mir-326-5p targeted LCN2 and repressed its expression. (A) Real-time PCR analysis of LCN2 in OGD/R H9C2 transfected with mir-326-5p mimic or mir-326-5p inhibitor. (B) Western blot analysis of LCN2 in OGD/R H9C2 transfected with mir-326-5p mimic and mir-326-5p inhibitor. (C) Immunofluorescence staining of LCN2 in H9C2 transfected with mir-326-5p mimic or mir-326-5p inhibitor. (D) Luciferase activity of WT-LCN2 and MUT-LCN2 binding with mir-326-5p mimic. (E) Real-time PCR analysis of mir-326-5p in H9C2 of control, OGD/R and OGD/R + DFO group. (F) Real-time PCR analysis of LCN2 in H9C2 of control, OGD/R and OGD/R + DFO group. (G) Western blot analysis of LCN2 in H9C2 of in H9C2 of control, OGD, OGD/R and OGD/R + DFO group.

Data are expressed as mean ± SD (n = 3); *P < 0.05, **P < 0.01, ***P < 0.001.

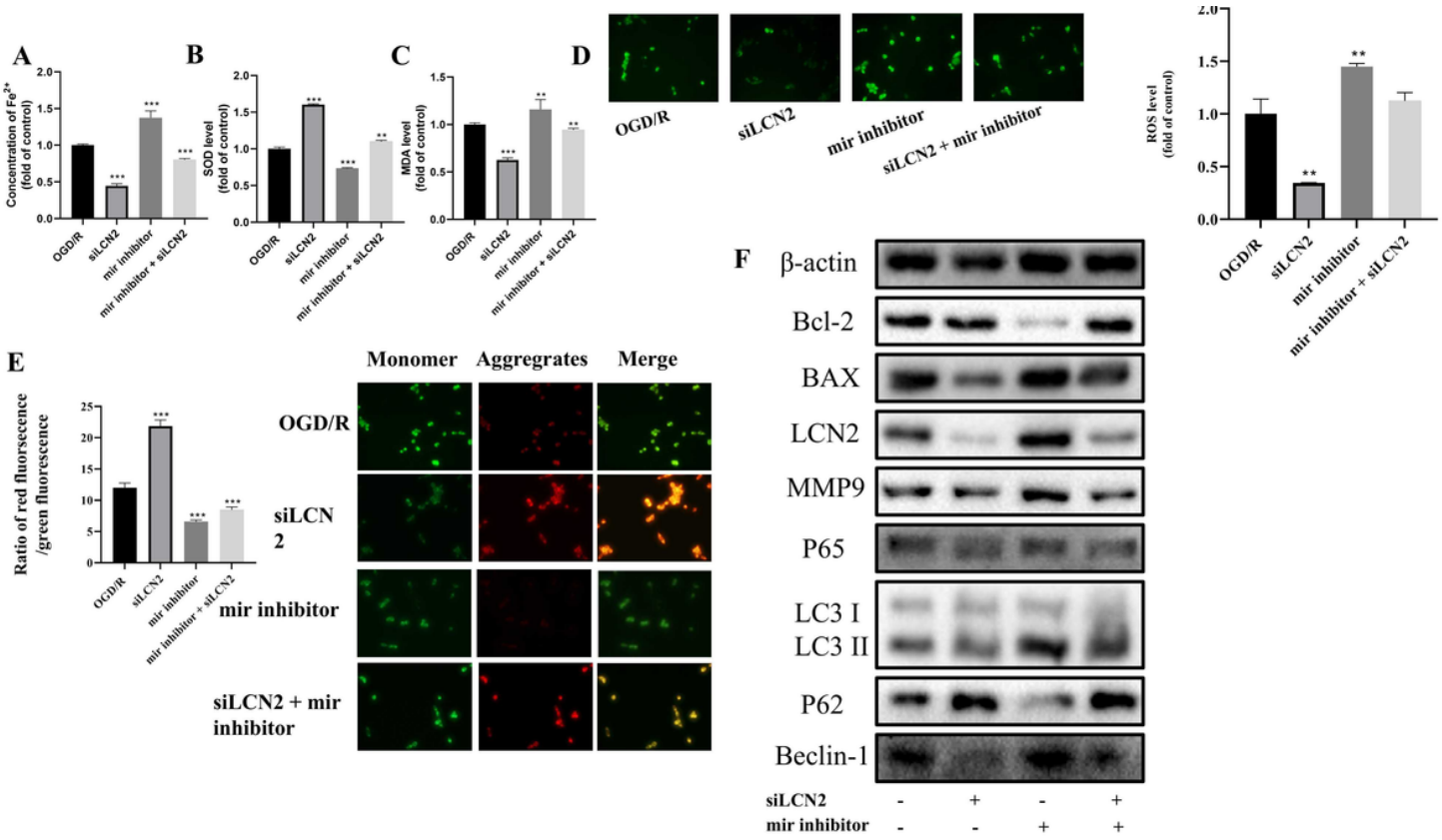

Figure 4

Axis of mir-326-5p/LCN2 regulated ferroptosis, autophagy and inflammatory response in OGD/R H9C2. (A) Detection of Fe2+ concentration in OGD/R H9C2 treated with LCN2 siRNA and mir-326-5p inhibitor. (B) Detection of SOD level in OGD/R H9C2 treated with LCN2 siRNA and mir-326-5p inhibitor. (C) Detection of MDA level in OGD/R H9C2 treated with LCN2 siRNA and mir-326-5p inhibitor. (D)Fluorescence staining of ROS in OGD/R H9C2 treated with LCN2 siRNA and mir-326-5p inhibitor. (E)Fluorescence staining of JC-1 in OGD/R H9C2 treated with LCN2 siRNA and mir-326-5p inhibitor. (green fluorescent represents JC-1 monomers and red fluorescent represents JC-1 aggregate forms). (F) Western blot analysis of LCN2, Bcl-2, Bax, MMP9, p65, Beclin-1, p62 and LC3 I/II in OGD/R H9C2 treated with LCN2 siRNA and mir-326-5p inhibitor.

Data are expressed as mean ± SD (n = 3); *P < 0.05, **P < 0.01, ***P < 0.001.

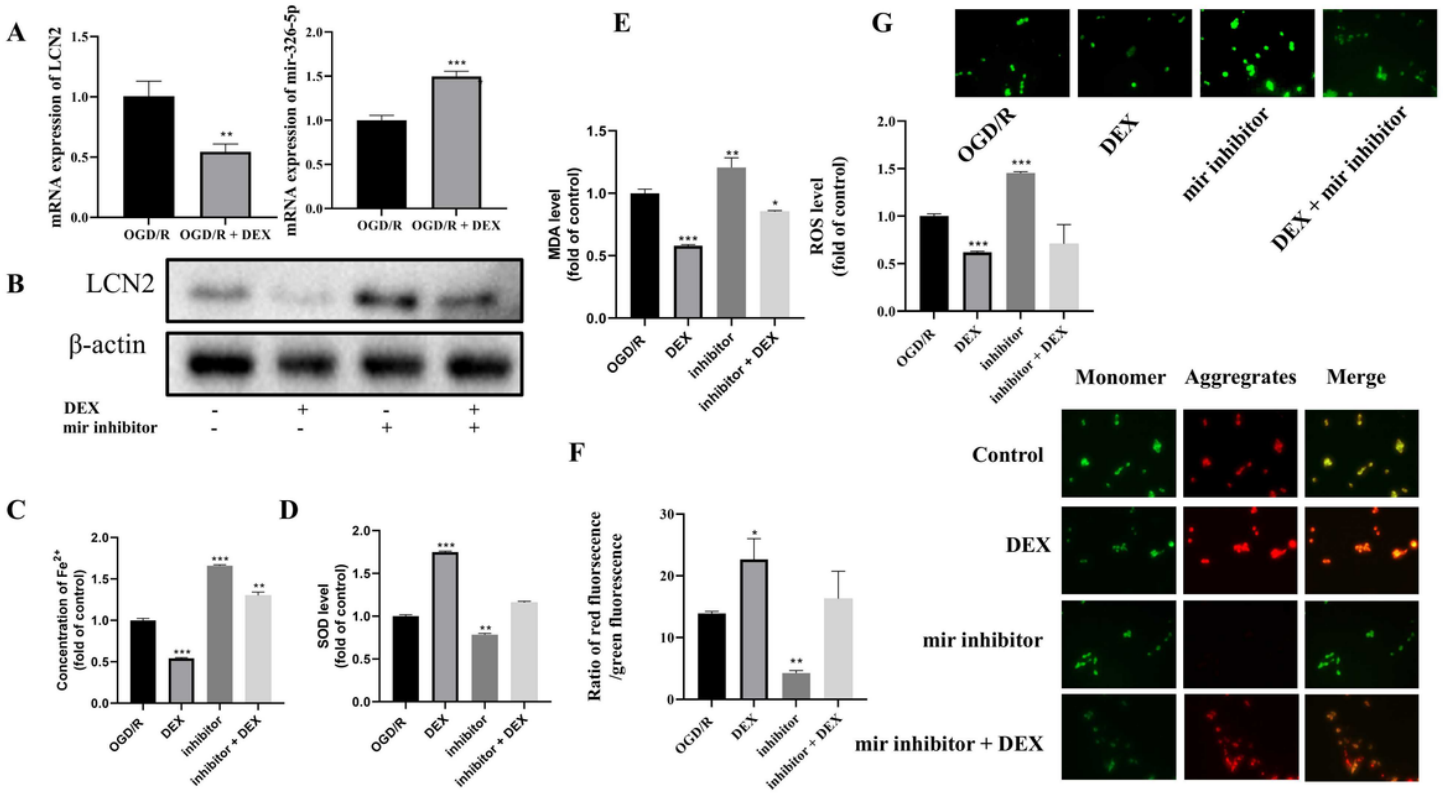

Figure 5

DEX treatment attenuated ferroptosis via mir-326-5p/LCN2 axis. (A) Real-time PCR analysis of mir-326-5p and LCN2 in OGD/R H9C2 and OGD/R H9C2 treated with DEX. (B) Western blot analysis of LCN2 in OGD/R H9C2 treated with DEX and mir-326-5p inhibitor. (C) Detection of Fe2+ concentration in OGD/R H9C2 treated with DEX and mir-326-5p inhibitor. (D) Detection of SOD level in OGD/R H9C2 treated with DEX and mir-326-5p inhibitor. (E) Detection of MDA level in OGD/R H9C2 treated with DEX and mir-326-5p inhibitor. (F)Fluorescence staining of ROS in OGD/R H9C2 treated with DEX and mir-326-5p inhibitor. (E)Fluorescence staining of mitochondrial membrane potential in OGD/R H9C2 treated with DEX and mir-326-5p inhibitor. (green fluorescent represents JC-1 monomers and red fluorescent represents JC-1 aggregate forms).

Data are expressed as mean ± SD (n = 3); *P < 0.05, **P < 0.01, ***P < 0.001.

Supplementary Files

This is a list of supplementary files associated with this preprint. Click to download.

- SupplementaryFig.1.jpg
- SupplementaryFig.2.jpg
- SupplementaryFig.3.jpg
- SupplementaryFig.4.jpg

- SupplementaryTable1.PrimersequencesforRTqPCR.docx
- Highlights.docx